



## Discovery and optimization of potent and selective triazolopyridazine series of c-Met inhibitors

Alessandro A. Boezio<sup>\*</sup>, Loren Berry, Brian K. Albrecht, David Bauer, Steven F. Bellon, Christiane Bode, April Chen, Deborah Choquette, Isabelle Dussault, Satoko Hirai, Paula Kaplan-Lefko, Jay F. Larrow, Min-Hwa Jasmine Lin, Julia Lohman, Michele H. Potashman, Karen Rex, Michael Santostefano, Kavita Shah, Roman Shimanovich, Stephanie K. Springer, Yohannes Teffera, Yajing Yang, Yihong Zhang, Jean-Christophe Harmange

Amgen Inc., One Kendall Square, Building 1000, Cambridge, MA 02139, USA  
Amgen Inc., One Amgen Center Drive, Thousand Oaks, CA 91320, USA

### ARTICLE INFO

#### Article history:

Received 8 July 2009  
Revised 22 September 2009  
Accepted 24 September 2009  
Available online 27 September 2009

#### Keywords:

Tyrosine kinase  
c-Met  
Triazolopyridazines  
TDI

### ABSTRACT

Deregulation of the receptor tyrosine kinase c-Met has been implicated in several human cancers and is an attractive target for small molecule drug discovery. We previously showed that O-linked triazolopyridazines can be potent inhibitors of c-Met. Herein, we report the discovery of a related series of N-linked triazolopyridazines which demonstrate nanomolar inhibition of c-Met kinase activity and display improved pharmacodynamic profiles. Specifically, the potent time-dependent inhibition of cytochrome P450 associated with the O-linked triazolopyridazines has been eliminated within this novel series of inhibitors. N-linked triazolopyridazine **24** exhibited favorable pharmacokinetics and displayed potent inhibition of HGF-mediated c-Met phosphorylation in a mouse liver PD model. Once-daily oral administration of **24** for 22 days showed significant tumor growth inhibition in an NIH-3T3/TPR-Met xenograft mouse efficacy model.

Published by Elsevier Ltd.

The receptor tyrosine kinase c-Met and its natural ligand, hepatocyte growth factor (HGF), are involved in cell proliferation, migration, and invasion and are essential for normal embryonic development.<sup>1</sup> Deregulation of c-Met/HGF signaling can lead to tumorigenesis and metastasis and has been implicated in a variety of cancers.<sup>2</sup> Several mechanisms lead to deregulation, including overexpression of c-Met and/or HGF, amplification of the MET gene, or activating mutations of c-Met, all of which have been found in human cancers.<sup>3</sup>

A small molecule inhibitor of c-Met has the potential of blocking both ligand-dependent and ligand-independent activity of c-Met and several approaches to intercept the HGF/c-Met pathway are currently being tested in the clinic.<sup>4</sup> We previously reported the discovery of a potent, orally active c-Met inhibitor for the treatment of cancer.<sup>5</sup> In an effort to design a novel chemotype with improved cellular potency and selectivity as a second generation inhibitor, we recently reported a series of O-linked triazolopyridazines (i.e., **1**) as potent and selective c-Met inhibitors.<sup>6</sup>

While inhibitors from this series demonstrated *in vivo* efficacy, metabolic profiling of these molecules revealed a tendency to inhibit cytochrome P450 3A4 (CYP3A4) in a time-dependent manner.<sup>7</sup>

Pre-incubation of compound **1** with human liver microsomes for 30 min resulted in an eightfold decrease in IC<sub>50</sub> for CYP3A4 metabolic activity relative to the IC<sub>50</sub> without preincubation (Fig. 1). Such a decrease in IC<sub>50</sub> indicated the presence of potent time-dependent inhibition (TDI).<sup>8</sup> Given that CYP3A4 accounts for 30% of total CYP protein in the human liver and is estimated to be involved in the metabolism of 50% of drugs used in humans, TDI of this enzyme presents concerns for drug–drug interactions in combination therapies in clinical oncology.<sup>9</sup> For this reason, we dedicated our efforts toward understanding and eliminating this liability.

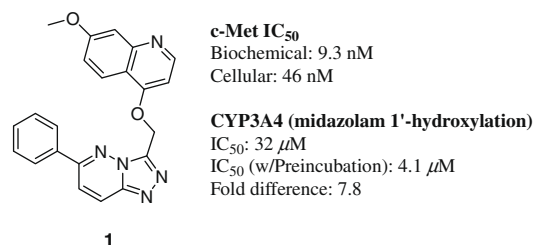


**Figure 1.** Representative example of a previously disclosed O-linked triazolopyridazine.

<sup>\*</sup> Corresponding author.

E-mail address: aboezio@amgen.com (A.A. Boezio).

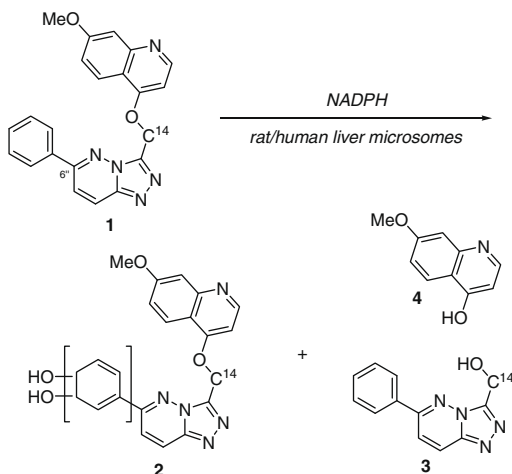
Inhibition of CYP isoenzymes is generally characterized as reversible or irreversible depending on the kinetics of the inhibition. Irreversible inhibition, or mechanism-based inhibition, of CYP is caused by the formation of a reactive metabolite that binds covalently within the active site of the enzyme, leading to TDI.<sup>7,10</sup> Therefore, in order to evaluate the potential for reactive metabolite formation and in turn the presence of irreversible CYP inhibition, <sup>14</sup>C-radiolabeled compound **1** was prepared and its metabolite profile was assessed. When <sup>14</sup>C-**1** was incubated in rat and human liver microsomes in the presence of NADPH two major metabolic pathways were identified (Scheme 1).

The first pathway involved the formation of a C-6' aryl dihydrodiol **2**, via a reactive epoxide intermediate and confirmed by a glutathione trapping experiment. The second pathway led to the formation of (6-phenyl-[1,2,4]triazolo[4,3-*b*]pyridazin-3-yl)methanol (**3**) and 7-methoxyquinolin-4-ol (**4**),<sup>11</sup> via O-dealkylation.

In an attempt to prevent the formation of reactive metabolites, efforts were directed at altering the metabolic profile of **1**. Since reactive epoxide intermediates are known to often lead to TDI,<sup>12</sup> our initial work focused on modifying the C-6' aryl group to prevent the formation of diol **2**. To this end, analogs **5–8** wherein aryl fluorides or a heterocycle were incorporated at the C-6' position were analyzed for their potential to inhibit CYP3A4 in a time-dependent manner. As illustrated in Table 1, these modifications did not translate to a consistent reduction in TDI of CYP3A4.

We then directed our efforts toward the second metabolic path.<sup>13</sup> Initial efforts involved increasing the steric bulk by introducing chirality at the methylene bridge of the tether, as exemplified by enantiomers **9** and **10** (Table 2). While this modification decreased affinity for the enzyme (104 nM and 236 nM, respectively), it led to a modest reduction in the TDI of CYP3A4. More promising results were obtained upon modifying the two atom tether linking the triazolopyridazine and the quinoline moieties. Thus, replacement of the oxygen tether in **1** with either nitrogen or sulfur provided compounds **11** and **12**. The c-Met inhibitory activity of both **11** and **12** was substantially reduced in comparison to **1**; however, complete reduction of time-dependent inhibition of CYP3A4 was observed in both compounds.

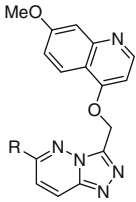
Having identified triazolopyridazines that lacked TDI, attention was shifted to improving the c-Met inhibitory activity of N-linked triazolopyridazine **11**. The loss of potency observed between **1** and **11** could be rationalized using the co-crystal structure of **1** bound to the unphosphorylated c-Met kinase domain. Based on the conformation of **1** in the active site of c-Met (Fig. 2),<sup>15</sup> it

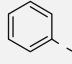
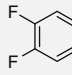
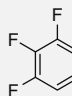
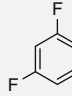
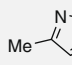


Scheme 1. Identification of the pathways involved in the metabolism of **1**.

Table 1

O-Linked triazolopyridazines; c-Met potency and time-dependent inhibition of CYP3A4



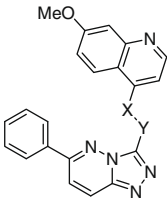
Compds	R	c-Met IC <sub>50</sub> <sup>a</sup> (nM)	CYP3A4 <sup>b</sup> IC <sub>50</sub> /IC <sub>50</sub> (w/Preinc.) (μM) fold difference
<b>1</b>		9	32/4.1 7.8
<b>5</b>		9	>50/6.4 >7.8
<b>6</b>		5	29/2.0 14
<b>7</b>		7	>50/8.3 >6.0
<b>8</b>		3	17/4.8 3.5

<sup>a</sup> Inhibition of kinase activity ( $n \geq 2$ ).

<sup>b</sup> Inhibition of CYP3A4 (midazolam 1'-hydroxylation) is represented by the fold difference or IC<sub>50</sub> shift with and without pre-incubation of the compound in the presence of NADPH.

Table 2

Triazolopyridazines; c-Met potency and time-dependent inhibition of CYP3A4



Compds	X	Y	c-Met IC <sub>50</sub> <sup>a</sup> (nM)	CYP3A4 <sup>b</sup> IC <sub>50</sub> /IC <sub>50</sub> (w/Preinc.) (μM) fold difference
<b>1</b>	O	CH <sub>2</sub>	9	32/4.1 7.8
<b>9</b>	O	CHMe (S) <sup>14</sup>	104	14/3.9 3.6
<b>10</b>	O	CHMe (R)	236	18/8.9 2.0
<b>11</b>	NH	CH <sub>2</sub>	1366	>50/50 >1.0
<b>12</b>	S	CH <sub>2</sub>	>6667	4.5/7.0 0.64

<sup>a</sup> Inhibition of kinase activity ( $n \geq 2$ ).

<sup>b</sup> Inhibition of CYP3A4 (midazolam 1'-hydroxylation) is represented by the fold difference or IC<sub>50</sub> shift with and without pre-incubation of the compound in the presence of NADPH.

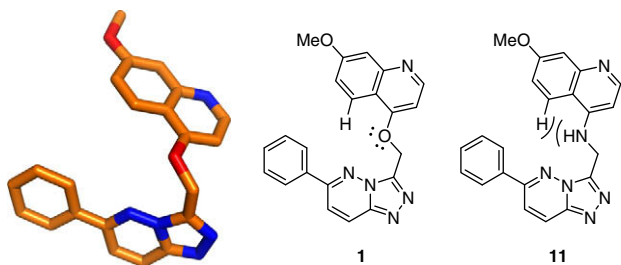


Figure 2. Binding conformation of **1** in the active site of c-Met.

was hypothesized that compound **11** would bind in such a manner that a repulsive interaction would exist between the amine hydrogen of the tether and the hydrogen at the C-5 position of the quinoline.

To test this hypothesis, naphthyridine **13**, where the CH in the 5-position of the quinoline in **11** was replaced with a nitrogen, was synthesized. As predicted, incorporation of the naphthyridine moiety led to the complete restoration of the enzymatic c-Met inhibitory activity. Moreover, the enzymatic to cellular c-Met potency shift displayed by **1** (9 vs 46 nM) was completely reduced in naphthyridine **13** (17 vs 14 nM). Finally, we were also encouraged to see **13** did not demonstrate time-dependent inhibition of CYP3A4.

Examination of the crystal structure of **13** within the catalytic domain of unphosphorylated c-Met revealed that the inhibitor assumed a 'U-shaped' binding mode with the inhibitor wrapped around Met1211 (Fig. 3).<sup>16</sup> An intramolecular hydrogen bond between the NH of the tether and the N-5 naphthyridine exists and serves to maintain this binding mode. As illustrated, the naphthyridine ring participates in a three point binding interaction with the backbone of Met1160 and Pro1158 of the hinge region. N-1 of the triazolopyridazine interacts with the backbone NH of Asp1222 and an additional two point binding exists between C-7' and C-2'' of **13**

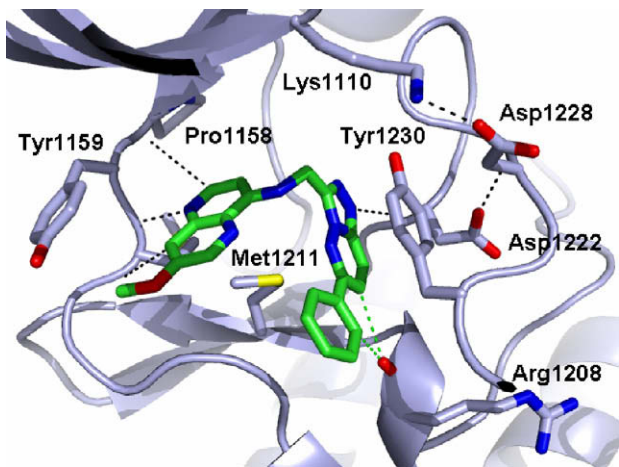
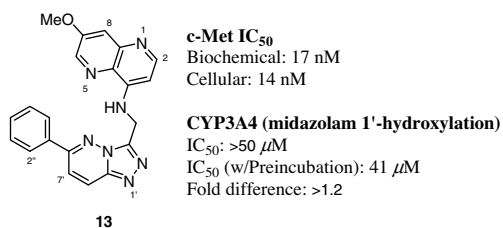
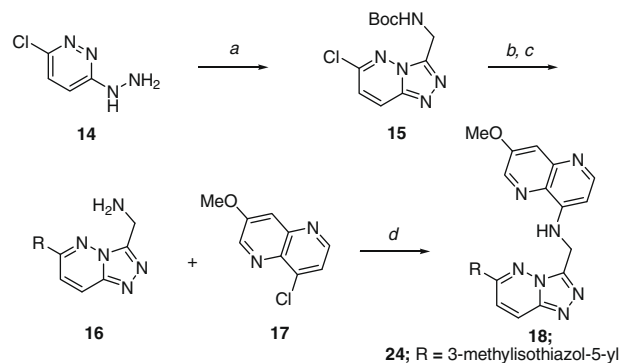


Figure 3. Crystal structure of c-Met+triazolopyridazine **13**.

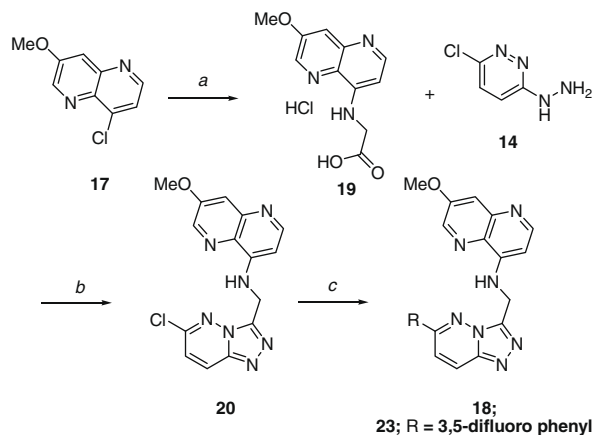


Scheme 2. Reagents and conditions: (a) Boc-glycine, CDI, MeCN, 0 °C; then *p*-TsOH, reflux, 82%; (b) 3-methyl-5-(trimethylstannyl)isothiazole, Pd(OAc)<sub>2</sub>, XPhos, *p*-dioxane, 90 °C, 33%; Pd/ligand (PdCl<sub>2</sub>(dppf)-DCM, Pd(OAc)<sub>2</sub>/X-Phos), RM (M = B(OR')<sub>2</sub>; SnR'<sub>3</sub>; ZnX), solvent (DMF, *p*-dioxanes/water), T °C (80–140 °C), (29–81%); (c) TFA, DCM, rt; 82% (78–95%); (d) 2-BuOH, 120 °C (thermal) or 140 °C (μW), 62% (43–78%).

sharing both lone pairs of the carbonyl of Arg1208. Finally, a  $\pi$ -stacking interaction is present between the triazolopyridazine core and Tyr1230.

Based on the previous O-linked series (i.e., **1**), it was anticipated that the potency and PK would be improved by varying the C-6' aryl portion of the inhibitor.<sup>6</sup> Two unique synthetic routes were established, both of which were amenable to the late stage introduction of aryl groups at the C-6' position (Scheme 2). The first route began by coupling Boc-glycine and 3-chloro-6-hydrazinopyridazine **14** in the presence of CDI, followed by acid mediated cyclization. Triazolopyridazine chloride **15** participated in a variety of palladium-catalyzed cross-coupling reactions to afford analog **16** after deprotection under acidic conditions. The coupling of the triazolopyridazine **16** and naphthyridine **17**<sup>17</sup> fragments was accomplished via a thermal nucleophilic aromatic substitution to yield N-linked triazolopyridazines such as **18**.

The second synthetic approach (Scheme 3) began with a nucleophilic aromatic substitution with glycine *t*-butyl ester and 4-chloro-7-methoxynaphthyridine (**17**), followed by acidic cleavage of the acid *t*-butyl protecting group to provide **19**. HATU-mediated coupling of **19** with 1-(6-chloropyridazin-3-yl) hydrazine (**14**)



Scheme 3. Reagents and conditions: (a) (i) Glycine *t*-butyl ester hydrochloride, 2-BuOH, 100 °C; (ii) HCl (1 N), 80 °C, 75% after two steps; (b) (i) HATU, iPr<sub>2</sub>NEt, DMF, rt; (ii) *p*-TsOH, MeOH, 55 °C, 61% after two steps; (c) Cs<sub>2</sub>CO<sub>3</sub>, 3,5-difluorophenylboronic acid, PdCl<sub>2</sub>(dppf)-DCM, *p*-dioxane/water, 100 °C, 20%; Pd/ligand (PdCl<sub>2</sub>(dppf)-DCM, Pd(OAc)<sub>2</sub>/X-Phos), RM (M = B(OR')<sub>2</sub>; SnR'<sub>3</sub>; ZnX), solvent (DMF, *p*-dioxanes/water), T °C (80–140 °C), (20–62%).

followed by cyclization under mild acidic conditions furnished **20**. Finally, the triazolopyridazine chloride proved to be an effective coupling partner in a variety of palladium-mediated coupling reactions to generate analogs such as **18**.

Using the aforementioned synthetic routes, a series of triazolopyridazines was synthesized and evaluated.<sup>18</sup> Table 3 illustrates the biochemical and cellular potency against c-Met, as well as the CYP3A4 time-dependent inhibition potency (IC<sub>50</sub> shift). Compounds **21–24** were more potent on c-Met than **13** and demonstrated no enzyme to cell shift. We were also gratified to see a significant reduction in the CYP3A4 IC<sub>50</sub> shift in this new series of compounds **13**, **21–24**.

On the basis of their *in vitro* potencies and low TDI, the metabolic stability and pharmacokinetic profiles of 3,5-difluoro phenyl analog **23** and methylisothiazole **24** were further evaluated (Table 4). For both compounds, low intrinsic clearance across species and high plasma protein binding (PPB) were observed. Consistent with their low turnover in rat liver microsomes (RLM) and their high plasma protein binding, **23** and **24** were cleared at a low rate after dosing in male Sprague-Dawley rats. Furthermore, both compounds demonstrated acceptable bioavailability and suitable half-lives for further *in vivo* testing.

Both compounds were examined in a binding assay to assess the potential inhibition of the hERG potassium channel. Compound **23** was determined to have a K<sub>i</sub> of 0.2 μM while compound **24** was

less potent and demonstrated a K<sub>i</sub> of 1.6 μM. Although the hERG K<sub>i</sub> was significantly higher for compound **24**, the cardiovascular liability associated with potassium channel may be comparable to **23**, since the free fraction (*f<sub>u</sub>*) of **24** was found to be higher across species. To further evaluate possible cardiovascular liability, compound **24** was then evaluated in isolated rabbit heart. No significant change in electrocardiographic (ECG) parameters was found up to 3 μM.<sup>19</sup>

Before assessing the *in vivo* pharmacological activity of **24**, it was screened for inhibitory activity against an extensive panel of kinases. As shown in Figure 4, compound **24** demonstrated exquisite selectivity against a range of tyrosine and serine/threonine kinases.

The *in vivo* inhibitory activity of compound **24** on HGF-mediated c-Met phosphorylation was assessed in mouse liver (Fig. 5).<sup>5,6,20</sup> Compound **24** was administered at 30 mg/kg by oral gavage and HGF-induced c-Met phosphorylation was quantified at various time points thereafter. Compound **24** was potent in this assay with an approximate EC<sub>90</sub> of 136 nM in plasma and 1.8 μM in liver 6 h after compound administration. Moreover, **24** showed sustained inhibition of c-Met phosphorylation (>50%) up to 12 h.

To evaluate on mechanism tumor growth inhibition, compound **24** was assessed for its antitumor activity in a c-Met driven xenograft model (Fig. 6). The NIH-3T3/TPR-Met model derived from NIH3T3 cells transfected with human TPR-Met, an oncogenic form of c-Met, was employed in this study.<sup>20</sup> Following oral administration (q.d.) of **24** at 3, 10, 30 and 100 mg/kg over 22 days, dose-dependent tumor growth inhibition was observed with an ED<sub>50</sub> of approximately 3.3 mg/kg and an ED<sub>90</sub> of approximately 22 mg/kg with no adverse effect on body weight.

In conclusion, metabolite identification and analysis of structure-CYP TDI relationship allowed us to considerably reduce the TDI liability previously observed in compounds **1** and **5–8**. Several analogs of this new series of inhibitors were prepared and were shown to demonstrate excellent potency against c-Met. Compound **24** exhibited a favorable pharmacokinetic profile, and demonstrated a strong correlation between inhibition of HGF-mediated c-Met phosphorylation in mouse liver and plasma drug concentration. Furthermore, **24** completely inhibited the growth of a c-Met dependent human tumor model.

**Table 3**

N-Linked triazolopyridazines; c-Met inhibition and time-dependent inhibition of CYP3A4

Compds	R	c-Met IC <sub>50</sub>	CYP3A4 <sup>c</sup>
		Biochemical <sup>a</sup> /cellular <sup>b</sup> (nM)	IC <sub>50</sub> /IC <sub>50</sub> (w/Preinc.) (μM) fold difference
<b>13</b>		17/14	>50/41 >1.2
<b>21</b>		9/7	>50/9.1 >5.5
<b>22</b>		5/7	>50/16 >3.1
<b>23</b>		5/3	>50/29 >1.7
<b>24</b>		5/3	>50/26 >1.9

<sup>a</sup> Inhibition of kinase activity (*n* ≥ 2).

<sup>b</sup> Inhibition of HGF-mediated c-Met phosphorylation in PC3 cells (*n* ≥ 2).

<sup>c</sup> Inhibition of CYP3A4 is represented by the fold difference or IC<sub>50</sub> shift with and without pre-incubation of the compound in the presence of NADPH.

**Table 4**

Pharmacokinetic profile of selected compounds

	<b>23</b>	<b>24</b>
RLM (Cl <sup>a</sup> , μL/min/mg)	53	59
MLM (Cl <sup>a</sup> , μL/min/mg)	49	60
HLM (Cl <sup>a</sup> , μL/min/mg)	47	24
PPB (%) <sup>b</sup> Rat	99.8	99.3
Mouse	97.7	93.6
Human	99.2	97.5
<i>Rat pharmacokinetics<sup>c</sup></i>		
Cl, (L/h/kg)	0.043 <sup>d</sup>	0.185 <sup>e</sup>
V <sub>ss</sub> , (L/Kg)	0.201 <sup>d</sup>	0.303 <sup>e</sup>
T <sub>1/2</sub> , (h)	3.84 <sup>d</sup>	1.76 <sup>e</sup>
AUC <sub>0→∞</sub> , (ng h/mL)	31,100 <sup>f</sup>	3500 <sup>f</sup>
F, (%)	62 <sup>f</sup>	30.5 <sup>f</sup>

<sup>a</sup> *In vitro* (RLM = rat liver microsomes; MLM = mouse liver microsomes; HLM = human liver microsomes).

<sup>b</sup> Separation method = equilibrium dialysis; concentration = 5 μg/mL.

<sup>c</sup> *In vivo* experiments were carried out with male Sprague-Dawley rats *n* = 3.

<sup>d</sup> *iv*, 0.25 mg/kg (DMSO).

<sup>e</sup> *iv*, 0.25 mg/kg (20% hydroxypropyl beta-cyclodextrin in water pH 3.5 w/MSA).

<sup>f</sup> *po*, 2 mg/kg (2% HMPC, 1% Tween in water pH 2.2 w/HCl).

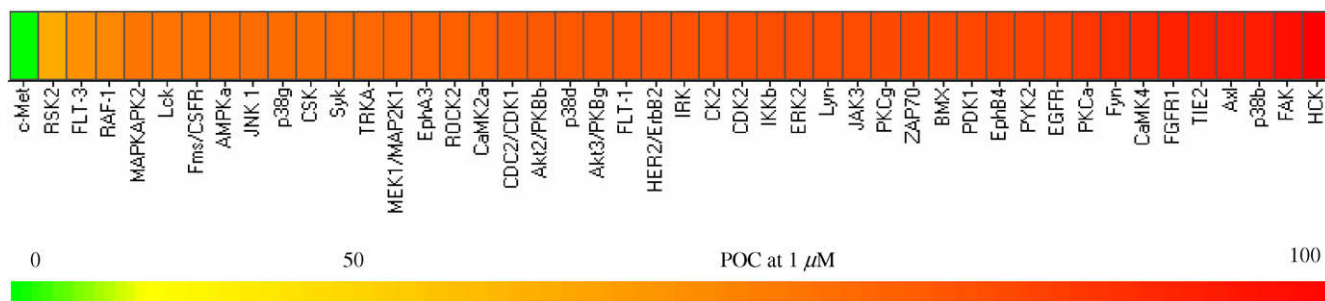


Figure 4. Selectivity heat map for compound 24.

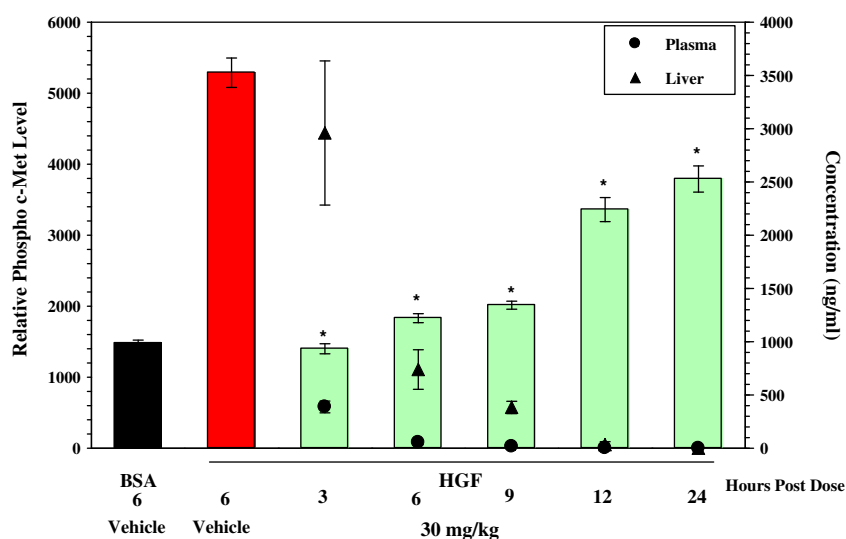


Figure 5. Effect of **24** administered by oral gavage on HGF-mediated c-Met phosphorylation in mice over time. Asterisk denotes  $p < 0.0001$  compared with the HGF group (red bar). Bars represent the mean  $\pm$  standard deviation ( $n = 3$ ). Circles represent mean plasma and triangles represent mean liver concentrations  $\pm$  standard deviation. (Vehicle: 2% HMPC, 1% Tween in water pH 2.2 w/MSA).

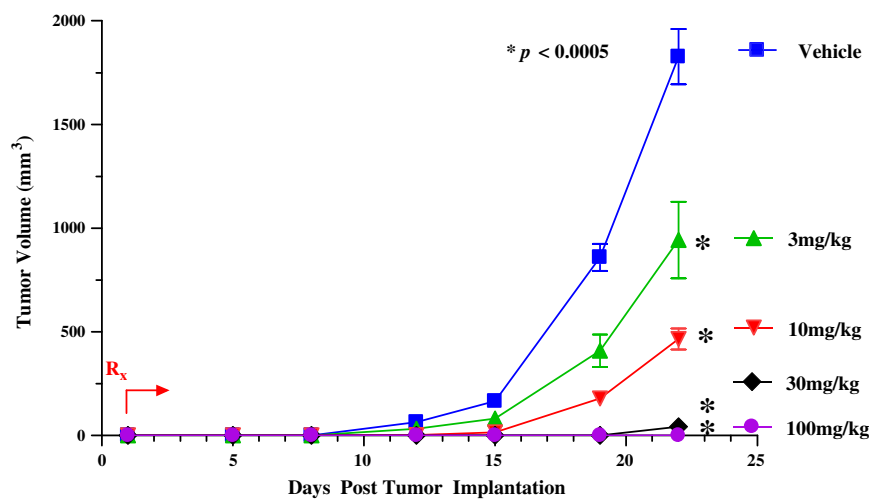


Figure 6. Effect of **24** on tumor growth inhibition in the NIH-3T3/TPR-Met xenograft model. Compound **24** was administered by oral gavage once per day beginning 24 h post tumor cell implantation. Results are expressed as mean  $\pm$  standard error ( $n = 12$  per group). Asterisk denotes  $p < 0.0005$  compared to treatment with vehicle. The  $AUC_{(0-24)}$  at  $ED_{50}$  and  $ED_{90}$  were 0.43 and 4.7  $\mu M h$ , respectively. (Vehicle: 2% HMPC, 1% Tween in water pH 2.2 w/MSA).

## Acknowledgments

The authors thank Katrina Copeland, Matthew Martin and Matt Weiss for their editing work, Doug Whittington for crystallographic assistance, Joanna Balsamo and Josh Toschi for in vivo formulation preparations and Monica Reese for technical assistance with mouse models.

## References and notes

- Giordano, S.; Ponzetto, C.; Di Renzo, M. F.; Cooper, C. S.; Comoglio, P. M. *Nature* **1989**, *339*, 155.
- Birchmeier, C.; Birchmeier, W.; Gherardi, E.; Met, G. F. *Nat. Rev. Mol. Cell Biol.* **2003**, *4*, 915.
- Dharmawardana, P. G.; Giubellino, A.; Bottaro, D. P. *Curr. Mol. Med.* **2004**, *4*, 855.
- Small molecules: Cui, J. J. *Exp. Opin. Ther. Pat.* **2007**, *17*, 1035; Biologicals: Cao, B.; Su, Y.; Oskarsson, M.; Zhao, P.; Kort, E. J.; Fisher, R. J.; Wang, L. M.; Vande Woude, G. F. *Proc. Natl. Acad. Sci. U.S.A.* **2001**, *98*, 7443.
- Liu, L.; Siegmund, A.; Xi, N.; Kaplan-Lefko, P.; Rex, K.; Chen, A.; Lin, J.; Moriguchi, J.; Berry, L.; Huang, L.; Teffera, Y.; Yang, Y.; Zhang, Y.; Bellon, S. F.; Lee, M.; Shimanovich, R.; Bak, A.; Dominguez, C.; Norman, M. H.; Harmange, J.-C.; Dussault, I.; Kim, T.-S. *J. Med. Chem.* **2008**, *51*, 3688.
- Albrecht, B. K.; Harmange, J.-C.; Bauer, D.; Berry, L.; Bode, C.; Boezio, A. A.; Chen, A.; Choquette, D.; Dussault, I.; Fridrich, C.; Hirai, S.; Hoffman, D.; Larrow, J. F.; Kaplan-Lefko, P.; Lin, J.; Lohman, J.; Long, A. M.; Moriguchi, J.; O'Connor, A.; Potashman, M. H.; Reese, M.; Rex, K.; Siegmund, A.; Shah, K.; Shimanovich, R.; Springer, S. K.; Teffera, Y.; Yang, Y.; Zhang, Y.; Bellon, S. F. *J. Med. Chem.* **2008**, *51*, 2879.
- Zhou, S.; Chan, S. Y.; Goh, B. C.; Chan, E.; Duan, W.; Huang, M.; McLeod, H. L. *Clin. Pharmacokinet.* **2005**, *44*, 279.
- Berry, L. M.; Zhao, Z. *Drug Metab. Lett.* **2008**, *2*, 51.
- Zhou, S.; Chan, E.; Li, X.; Huang, M. *Ther. Clin. Risk Manag.* **2005**, *1*, 3.
- The mechanism of TDI has not been determined in that series of compounds.
- Minor signal by mass spectrometry but not quantifiable by radiochromatogram due to the loss of the  $^{14}\text{C}$  label.
- Fontana, E.; Dansette, P. M.; Poli, S. M. *Curr. Drug. Metab.* **2005**, *6*, 413; Kalgutkar, Amit S.; Obach, Scott R.; Maurer, Tristan S. *Curr. Drug Metab.* **2007**, *8*, 407.
- This position was also targeted by a minor intrinsic reactivity by glutathione: Teffera, Y.; Colletti, A. E.; Harmange, J.-C.; Hollis, L. S.; Albrecht, B. K.; Boezio, A. A.; Liu, J.; Zhao, Z. *Chem. Res. Toxicol.* **2008**, *21*, 2216.
- The absolute stereochemistry was assigned by co-crystallization of **9** in favor of **10** from a racemic mixture of **9/10** with unphosphorylated c-Met.
- Protein removed for clarity.
- PDB deposition code number for the crystal structure of c-Met+**13** is 315 N.
- Albrecht, B.; Bauer, D.; Bellon, S.; Bode, C.; Booker, S.; Boezio, A.; Choquette, D.; D'Amico, D.; Harmange, J.-C.; Hirai, S.; Hungate, R.; Kim, T.-S.; Lewis, R.; Liu, L.; Lohman, J.; Norman, M.; Potashman, M.; Siegmund, A.; Springer, S.; Stec, M.; Xi, N.; Yang, K. Preparation of fused heterocyclic derivatives for treating HGF-mediated diseases. *PCT Int. Appl.* **2008**, pp 310, WO 2008008539.
- Structure–activity relationship is similar across both series (O vs N-linked) with respect to potency and pharmacokinetic profiles.
- Based on maximum solubility in the assay buffer.
- Zhang, Y.; Kaplan-Lefko, P. J.; Rex, K.; Yang, Y.; Moriguchi, J.; Osgood, T.; Mattson, B.; Coxon, A.; Reese, M.; Kim, T.-S.; Lin, J.; Chen, A.; Burgess, T. L.; Dussault, I. *Cancer Res.* **2008**, *68*, 6680; Park, M.; Dean, M.; Cooper, C. S.; Schmidt, M.; O'Brien, S. J.; Blaire, D. G.; Vande Woude, G. F. *Cell* **1986**, *45*, 895.